

NAVAL POSTGRADUATE SCHOOL Monterey, California



**Performance Evaluation of Antennas
Installed on a Joint Standoff Weapon (JSOW)
Captive Air Training Missile (CATM)**

by

D. C. Jenn

March 10, 1998

19980508 057

Approved for public release; distribution is unlimited.

Prepared for: NAVAIR PMA-201

DTIC QUALITY INSPECTED 4

NAVAL POSTGRADUATE SCHOOL
Monterey, California

RADM Robert C. Chaplin
Superintendent

R. Elster
Provost

This report was sponsored by NAVAIR PMA-201.

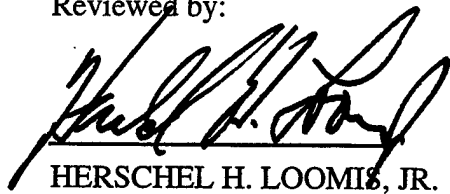
Approved for public release; distribution is unlimited.

The report was prepared by:



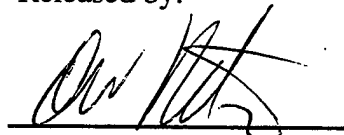
D. C. Jenn
Associate Professor
Department of Electrical and
Computer Engineering

Reviewed by:



HERSCHEL H. LOOMIS, JR.
Chairman
Department of Electrical and
Computer Engineering

Released by:



DAVID W. NETZER
Associate Provost and
Dean of Research

REPORT DOCUMENTATION PAGEForm Approved
OMB No. 0704-0188

Public reporting burden for the collection of information is estimated to average 1 hour per response, including the time for reviewing instructions, searching existing data sources, gathering and maintaining the data needed, and completing and reviewing the collection of information. Send comments regarding this burden estimate or any other aspect of this collection of information, including suggestions for reducing this burden to Washington Headquarters Services, Directorate for Information Operations and Reports, 1215 Jefferson Davis Highway, Suite 1204, Arlington VA 22202-4302, and to the Office of Management and Budget, Paperwork Reduction Project (0704-0188), Washington DC 20503.

1. AGENCY USE ONLY (Leave blank)	2. REPORT DATE March 10, 1998	3. REPORT TYPE AND DATES COVERED Technical Report	
4. TITLE AND SUBTITLE Performance Evaluation of Antennas Installed on a Joint Standoff Weapon (JSOW) Captive Carry Training Missile (CATM)		5. FUNDING NUMBERS 97110-T	
6. AUTHOR(S) D. C. Jenn			
7. PERFORMING ORGANIZATION NAME(S) AND ADDRESS(ES) Department of Electrical and Computer Engineering Naval Postgraduate School Monterey, CA 93943-5000		8. PERFORMING ORGANIZATION REPORT NUMBER NPS-EC-98-008	
9. SPONSORING/MONITORING AGENCY NAME(S) AND ADDRESS(ES) Program Executive Officer (TACAIR) Attn: PMA-201 (LCDR Mahr), Bldg. 2272 Ste. 448 47123 Buse Road, Unit IPT Patuxent River, MD 20670-1547		10. SPONSORING/MONITORING AGENCY REPORT NUMBER	
11. SUPPLEMENTARY NOTES The views expressed in this report are those of the author and do not reflect the official policy or position of the Department of Defense or the United States Government.			
12a. DISTRIBUTION/AVAILABILITY STATEMENT Approved for public release; distribution is unlimited.		12b. DISTRIBUTION CODE A	
13. ABSTRACT (Maximum 200 words) The captive air training missile (CATM) is a version of the joint standoff weapon (JSOW) that is to be used for training purposes. The CATM will be mounted on the wing of an F-18, yet its response to a control aircraft command must mimic that of the JSOW in free flight. The objective of this work is to determine the effect of the F-18 carriage aircraft on the performance of the CATM data link. Gain data was computed using APATCH for various CATM configurations and locations. The results indicate that there is significant degradation in the data link for mode 1 when $-90^\circ \leq AZ \leq 0^\circ$, $0^\circ \leq EL \leq 90^\circ$ and for mode 2 when $-90^\circ \leq AZ \leq 0^\circ$, all elevation angles. The performance is best when the CATM is located at the outer mount point on the wing.			
14. SUBJECT TERMS CATM, antennas		15. NUMBER OF PAGES 46	16. PRICE CODE
17. SECURITY CLASSIFICATION OF REPORT UNCLASSIFIED	18. SECURITY CLASSIFICATION OF THIS PAGE UNCLASSIFIED	19. SECURITY CLASSIFICATION OF ABSTRACT UNCLASSIFIED	20. LIMITATION OF ABSTRACT SAR

TABLE OF CONTENTS

I. INTRODUCTION	1
A. Background	1
B. Objective	1
C. Approach	4
II. COMPUTER CODES	5
A. Candidate Codes	5
B. CAD Model Generation	8
III. ANTENNA MODELS	13
IV. CAPTIVE CARRY PATTERN CHANGES	18
A. Description of the Calculated Data	18
B. Mode 1 Data	19
C. Mode 2 Data	20
V. CONCLUSIONS	20
VI. REFERENCES	21

I. INTRODUCTION

A. Background

The captive air training missile (CATM) is a version of the joint standoff weapon (JSOW) that is to be used for training purposes. The CATM will be mounted on the wing of an F-18, yet its response to a control aircraft command must mimic that of the JSOW in free flight. In order to simulate a wide range of operational scenarios, it is necessary that the captive configuration accommodate the corresponding weapon/control aircraft configurations. In the captive configuration, the line of sight between the weapon data link antenna and the control aircraft can be partially or completely blocked by the carriage aircraft surfaces as shown in Figure 1. This can result in degraded communication or possibly a short term total loss of signal. The extent of the degradation depends on the location of the CATM on the carriage aircraft and the relative geometry of the two aircraft.

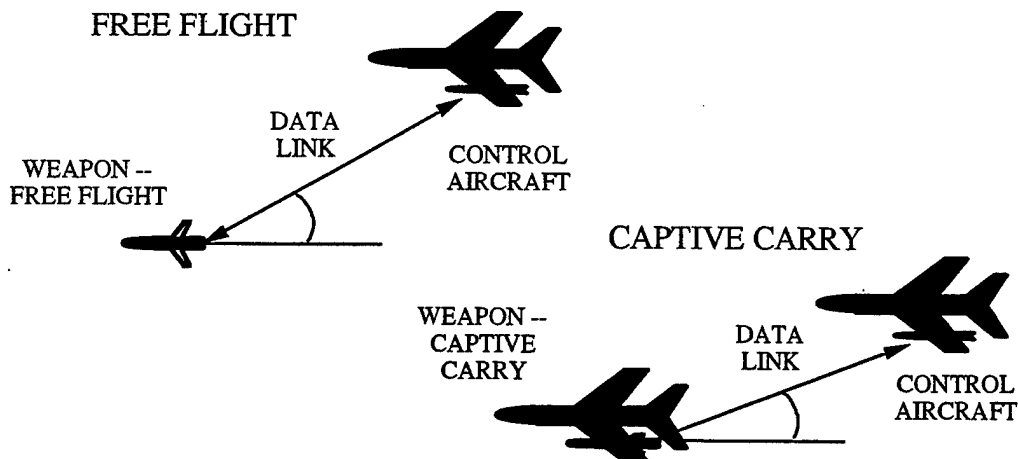


Figure 1: Illustration of the free flight and captive conditions.

B. Objective

The objective of this work is to determine the effect of the F-18 carriage aircraft on the performance of the weapon data link. For a weapon in free flight, the control aircraft has an unobstructed line of sight to the antenna. However, in the captive mode, the presence of the host aircraft can cause the line of sight to be blocked. Even if the line of sight is not completely blocked, several propagation paths between the weapon and control aircraft may exist as depicted in Figure 2. They include:

- 1) direct
- 2) reflection (single and multiple reflections)
- 3) diffraction
- 4) surface waves

If multiple signal paths exist, then constructive or destructive interference is possible (commonly referred to as multipath). For instance, a signal reflected from the wing could completely cancel with the direct signal under certain circumstances. This is an example of destructive interference, which can result in a loss of data. The relative strengths of these propagation mechanisms are determined by the frequency and the details of the weapon/control aircraft geometry.

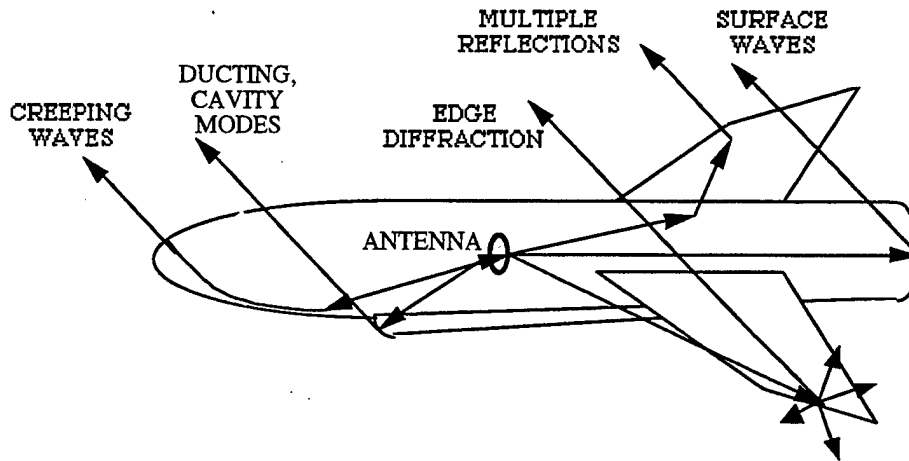


Figure 2: Illustration of several secondary scattering mechanisms that may occur due to the presence of the carriage aircraft.

If the control aircraft is transmitting to the JSAL pod (Figure 3), the power received by the pod due to the direct path is given by the Friis transmission equation [1]

$$P_{\text{dir}} = P_t G_t(\theta_t) G_r(\theta_r) \left(\frac{\lambda}{4\pi R} \right)^2 \quad (1)$$

where

- P_t = transmit power at the control aircraft
- P_{dir} = direct path received power at the weapon
- G_t = gain of transmit antenna in direction of weapon
- G_r = gain of receive antenna in direction of control aircraft
- R = range
- $\lambda = c/\lambda$ (c = speed of light)

The effects of multipath can be included in the power calculation by adding the contribution from each reflected path to the observer as shown in Figure 4 for a typical reflection. Thus, the total received power is

$$P_r = P_{\text{dir}} + P_{\text{ref}} \quad (2)$$

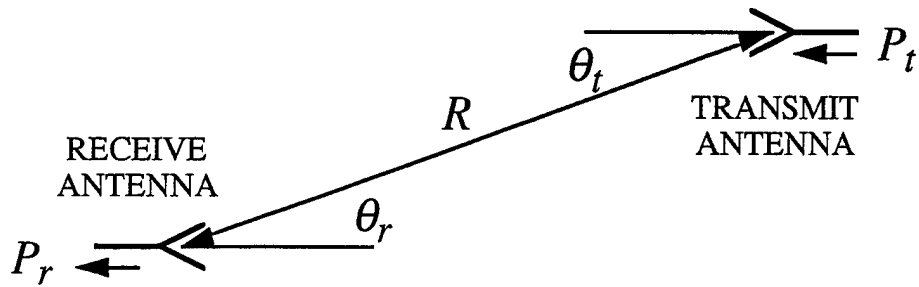


Figure 3: Direct transmission between the weapon and control aircraft.

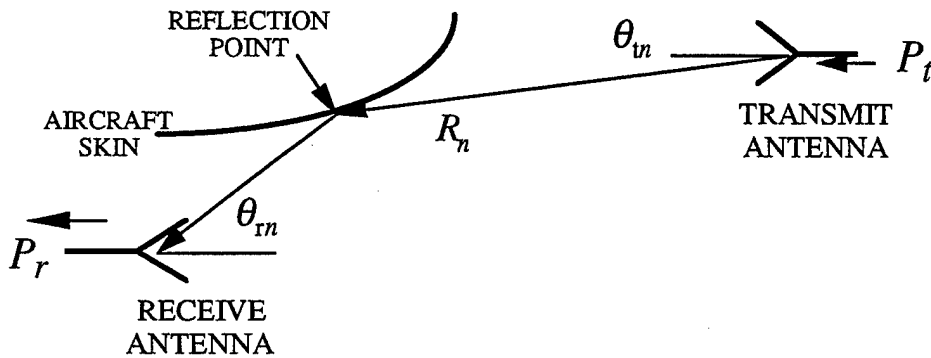


Figure 4: A typical reflection path between the weapon and control aircraft.

For N reflections

$$P_{\text{ref}} = P_t \sum_{n=1}^N G_t(\theta_{tn}) G_r(\theta_{rn}) \left(\frac{\lambda}{4\pi R_n} \right)^2 \exp(jk\Delta R_n) \Gamma_n \quad (3)$$

where

- $G_t(\theta_{tn})$ = gain of transmit antenna in direction of the n th reflection point
- $G_r(\theta_{rn})$ = gain of receive antenna in direction of the n th reflection point
- R_n = n th reflected path length
- ΔR_n = difference between the direct and n th reflected path lengths
- Γ_n = reflection coefficient for the n th reflection point

Reflection points on the aircraft dominate (i.e., ground reflections are of secondary importance), and therefore the reflection points are close to the antenna. If the observation point (control aircraft) is far from the CATM then the following approximations can be made:

1. In the denominator of Equation (3), $R_n \approx R$; however, this approximation is not valid in the argument of the exponential.
2. Since the antenna patterns are broad, the gain of the transmit antenna in the direct and reflected directions are nearly equal. Therefore, $G_t(\theta_n) = G_t(\theta)$ for all n .

Now Equation (2) can be written as

$$P_r = P_t G_t(\theta_t) \left(\frac{\lambda}{4\pi R_n} \right)^2 \underbrace{\left(1 + \sum_{n=1}^N G_r(\theta_n) \exp(jk\Delta R_n) \Gamma_n \right)}_{G_{\text{eff}}(\theta_r)} \quad (4)$$

where the summation can be interpreted as the CATM antenna effective gain in the presence of multipath. This is the gain that would be measured if the antenna and pod were installed on the aircraft and a conventional pattern measurement performed. Even though Equation (4) was derived on the basis of reflection, additional terms can be added for other scattering mechanisms.

C. Approach

The effective gain can be measured or computed using a computational electromagnetics (CEM) code. In both cases, the procedure is the same. First, the antenna on the isolated weapon was modeled and the antenna gain pattern computed over a complete range of pattern angles at selected frequencies. Next, the antenna and weapon were modeled in the captive configuration (weapon mounted on the wing of the F-18). The antenna gain was computed at the same angles as in the first step. Any change between the two gains can be attributed to the presence of the host F-18. Pattern data were generated for several weapon mount locations. The effect of the CATM length and the presence of a drop tank on the adjacent mount point were also investigated.

To summarize, the antenna investigation was comprised of the following steps:

1. Develop a CAD model for the F-18, CATM, and antenna. Three antennas must be modeled: the central helix and the two wide angle microstrip patches.
2. Verify the antenna models by comparison with measured data.
3. Generate data for the isolated antenna and weapon.

4. Generate data for the captive configuration. Investigate the effect of:

- a. pod length and location on pylon
- b. pylon location on wing
- c. the presence of other aircraft ordinance

Data was generated at several frequencies over the data link operating band.

II. COMPUTER CODES

A. Candidate Codes

Computational electromagnetics (CEM) codes can be used to model the effects of the host aircraft on the weapon antenna performance. As applied to antennas and electromagnetic systems (i.e., radar, communication, and electronic warfare systems), CEM codes can be divided into two broad categories. The first category are those used to perform detailed antenna design and analysis. Codes in this category must be able to predict the effects of subtle geometric and material variations on the antenna performance. They are generally used in the early stages of the antenna design process to perform tradeoff studies.

The second category of computer codes are those used to predict the antenna's performance when it is in its operational environment; that is, when installed on the platform with other objects near it or in its field of view. These codes must be able to adequately model the interfering objects, an ability which generally occurs at the expense of the detailed antenna modeling capability. This is not due to any shortcoming in the electromagnetic theory, but it is a computational limitation imposed by the need for computer memory or practical computation times. In the second case, the impact on system performance is usually described by the change in the antenna pattern relative to what it would be in the isolated environment.

When an antenna is installed on a platform, the antenna can illuminate a portion of the platform surface. Current is induced on the surface setting up a scattered field. The scattered field in turn illuminates the antenna, which affects the current distribution on the antenna, and hence the original field incident on the platform surface is changed. This coupling between the antenna and its environment generally has only a minor effect on the radiation pattern. However, antenna coupling with objects in its near field can significantly affect the input voltage standing wave ratio (which causes power to be reflected at the antenna input).

This research requires CEM codes of the second type. The performance of the antenna on a complex structure is of interest. (Complex structures are those with curved surfaces, edges, protrusions, and composite materials.) Several frequency domain

codes are applicable to this problem. They are broadly grouped into the categories of approximate and rigorous methods. The codes and their capabilities are summarized in Table 1.

NAME	TYPE	ADVANTAGES	DISADVANTAGES
PATCH (Sandia Labs)	rigorous (MM)	<ul style="list-style-type: none"> • all frequencies • surface impedance • wide range of excitations • open source code 	<ul style="list-style-type: none"> • computer limitations
NEC-BSC (Ohio State)	approximate (GTD & GO)	<ul style="list-style-type: none"> • fast solutions • geometry viewer 	<ul style="list-style-type: none"> • limited to high frequencies • crude geometry models • crude antenna models • some scattering mechanisms missing • no antenna/platform coupling
APATCH (Demaco)	approximate (PO & SBR)	<ul style="list-style-type: none"> • interfaces directly with ACAD • detailed target models possible 	<ul style="list-style-type: none"> • limited to high frequencies • no antenna/platform coupling • crude antenna models

MM = method of moments

GTD = geometrical theory of diffraction

SBR = shooting and bouncing rays

PO = physical optics

ACAD = advanced computer aided design

GO = geometrical optics

Table 1: Summary of capabilities of candidate CEM codes.

Method of moments (MM) codes reduce the electromagnetic equations for the induced current to a set of simultaneous equations that are solved using matrix methods. PATCH is a MM code that uses triangular subdomains [2]. To apply the MM technique the scattering target must be discretized into a collection of triangular facets. The MM procedure is used to compute the current flowing on each facet for a given excitation condition. The excitation is a plane wave if the antenna is receiving. Various types of current and voltage excitations can be applied to the antenna structure if the antenna is transmitting. Once the currents are determined, the radiated or received field is computed by an integration. When the antenna surfaces are included in the MM patch model, then all of the interactions between the antenna and platform are included in the computation of current.

The size of the structure relative to the wavelength determines the size of the matrix. Therefore, large targets cannot be analyzed at high frequencies because of computer memory limitations. MM is not practical for the given aircraft size and frequencies of interest for this problem. However, PATCH can be used to compute the patterns of the helix and microstrip antennas

[3]. The patterns can then be used in an approximate CEM code to predict the platform effects.

Approximate codes ignore the higher order coupling, or approximate the higher order contributions by a series of correction terms. Examples of this type of code are APATCH [4] and NECBSC [5]. APATCH combines the physical optics approximation (PO) with the shooting and bouncing ray (SBR) technique to estimate multipath effects. SBR is a hybrid method that is used extensively in the calculation of the radar cross section (RCS) of large targets at high frequencies. It combines geometrical optics (GO) and the surface equivalence principle [6], and can be supplemented by the physical theory of diffraction (PTD). Current distributions are determined from the trajectories of rays in a dense bundle. The current distributions can be used to:

1. initiate secondary rays to evaluate multiple reflections,
2. compute PTD fringe currents for edge diffraction contributions, and
3. compute the far scattered fields.

Currently this technique is the most accurate and flexible for computing the scattering from large complex targets such as aircraft with engine inlets and cockpits.

<u>Input File</u>	<u>Output File</u>
Antenna generating data	Ray tracing statistics
Single elements	Sector sweeps
Arrays of elements	Linear polarization
Pattern lookup table	Circular polarization
Geometry file	Complex field
Surfaces (reflection)	(magnitude and phase)
Edges (diffraction)	Pattern cuts
Materials	Horizontal
Observation angles	Vertical
Directivity calculation	
Define EM model	

Table 2: Summary of APATCH capabilities.

NECBSC is based entirely on microwave optics. GO provides a means of calculating the field reflected from a surface. The associated edge effects require a mathematical model for edge diffraction. The geometrical theory of diffraction (GTD) is such a ray based edge diffraction theory. For GTD, rays are hypothesized that obey diffraction laws similar to reflection laws. A diffraction coefficient is defined which depends on the edge geometry and polarization of the incident wave. Upon diffraction, the scattered field is given by the incident field times the diffraction coefficient. The diffracted wave follows prescribed straight line paths in free space. The total field at an observation point is the vector sum of all the reflected and diffracted fields arriving at that point.

The formulas of microwave optics are derived on the basis of infinite frequency ($\lambda \rightarrow \infty$), which implies an electrically large target. Ray optics is frequently used in situations that severely violate this restriction and still yield surprisingly good results. The major disadvantage of ray tracing is the bookkeeping required for a complex target. Also, radiation patterns frequently contain discontinuities because of blockage or missing higher order diffraction contributions.

APATCH is the preferred code because of the inclusion of higher order scattering mechanisms, and its compatibility with computer aided design (CAD) software.

B. CAD Model Generation

Facet models can be generated using a computer aided design program named ACAD (Advanced Computer Aided Design) [7]. ACAD can read files in the IGES (International Graphics Exchange Standard) format, and therefore is capable of using databases generated by all of the major commercial CAD programs such as Autocad or Versacad. The antenna and platform configurations are relatively easy to change using a CAD program, which simplifies investigations into the effect of antenna location and body material composition on antenna performance.

ACAD provides users with the ability to create and modify geometry in two- or three-dimensions. Users can choose to model geometry with wire frames, surfaces, or solids. ACAD is the primary tool used by Lockheed Fort Worth Company's Advanced Programs for configuration and subsystem design of new and existing aircraft programs. ACAD's primary role is the generation of geometry and some limited analysis. Much of the analysis performed within ACAD is geometrical analysis. For other types of analysis, ACAD generates interface files for transferring to groups who specialize in a particular analysis field such as Radar Cross Section (RCS), Aero, or Computational Fluid Dynamics (CFD).

Inputting data to ACAD is accomplished through one of many input modes available to the designer. ACAD models can be viewed orthographically or in perspective. At the heart of the ACAD system is the associative database. In an associative database, geometry is linked together in a relational structure that remembers parent/child dependencies. This type of database enables rapid modifications of geometry, since modifying one geometric element automatically adjusts its dependencies based on a set of predefined rules. For instance, changing a control spline of a fuselage will automatically regenerate any surface(s) built with the spline. In turn, any geometry that is associated to the fuselage surface (i.e., plane/curve and surface intersections, fillets) will automatically regenerate.

Table 3 contains more information on the types of commands available on ACAD Version 9.0.

The F-18 and CATM were built using ACAD. The auto-meshing capability was used to generate facet models which could be directly ported to APATCH for use in the pattern calculations. Figures 5 and 6 show the F-18 and CATM patch model with the pod mounted on the right wing at the outboard and inboard locations, respectively. Two mesh densities are shown. The fine mesh conforms more closely to the actual aircraft surface contour, whereas the coarse mesh requires significantly less computational time. It was found that the coarse mesh yields sufficiently accurate results because the surfaces illuminated by the antenna have relatively large radii of curvature relative to the wavelength.

<u>Transformations</u>	<u>Intersections</u>
Scale	Curve-curve
Translate	Curve-plane
Rotate	Curve-surface
Mirror	Plane-surface
Copy	Surface-surface
	Curve projections

<u>Display options</u>	<u>Drafting Utilities</u>
User defined layers	Break, trim and join curves
Blank on/off	Corner
Color, style and fonts	Grouping
Hidden lines, flat and Gouraud shading	Construction planes
Auxiliary viewing	Local coordinate systems
Orthographic and perspective viewing	Offsets
Multiple windows	Text and dimensions
Dynamic viewing	Groups, dittos and details
Zooming, panning and auto extents	Crosshatching

<u>Input options</u>	<u>Three-dimensional design</u>
Digitize	Point, line and splines
Reference existing data points	Conic, circles and ellipses
Key in coordinates	Six forms of surfaces
Intersection	Curve and surface editing
Point on	Trimmed surfaces
Snap to grid	Mass properties (volumes & areas)
Hierarchical input mode	Offset surfaces
	Wireframe, surfaces and solids

Table 3: Summary of ACAD capabilities.

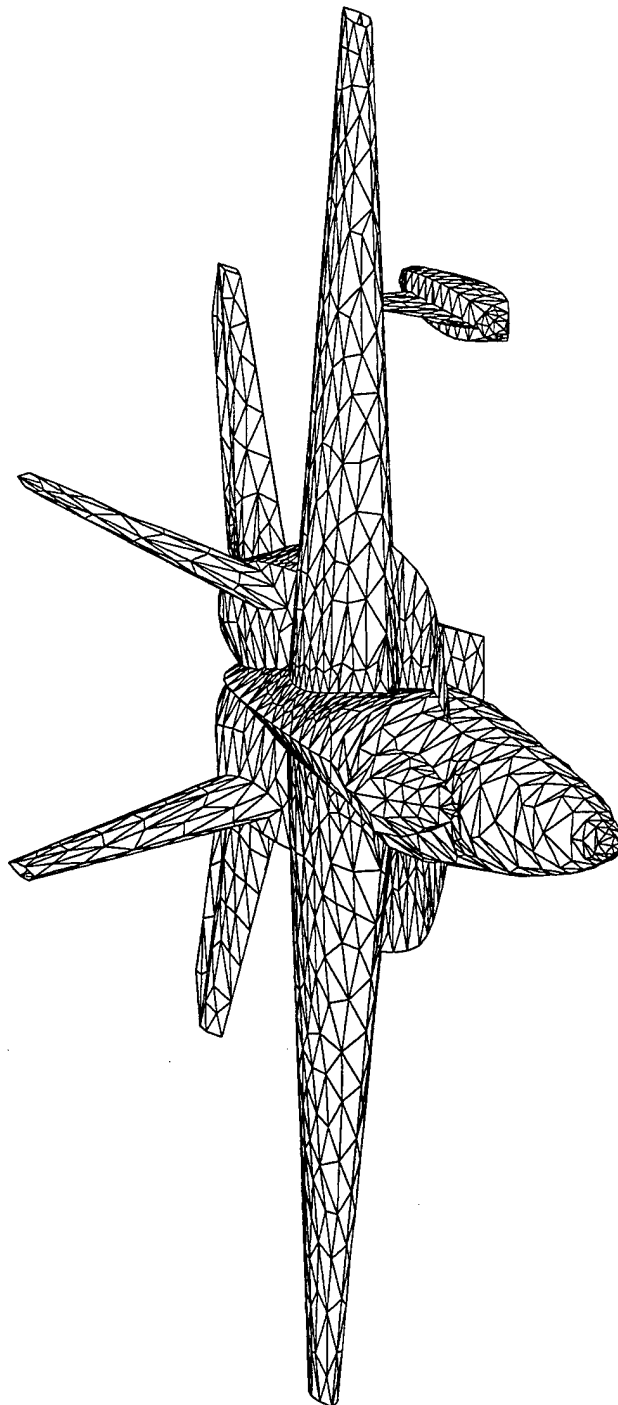


Figure 5: F-18 and CATM facet model built with ACAD (pod at outboard location).

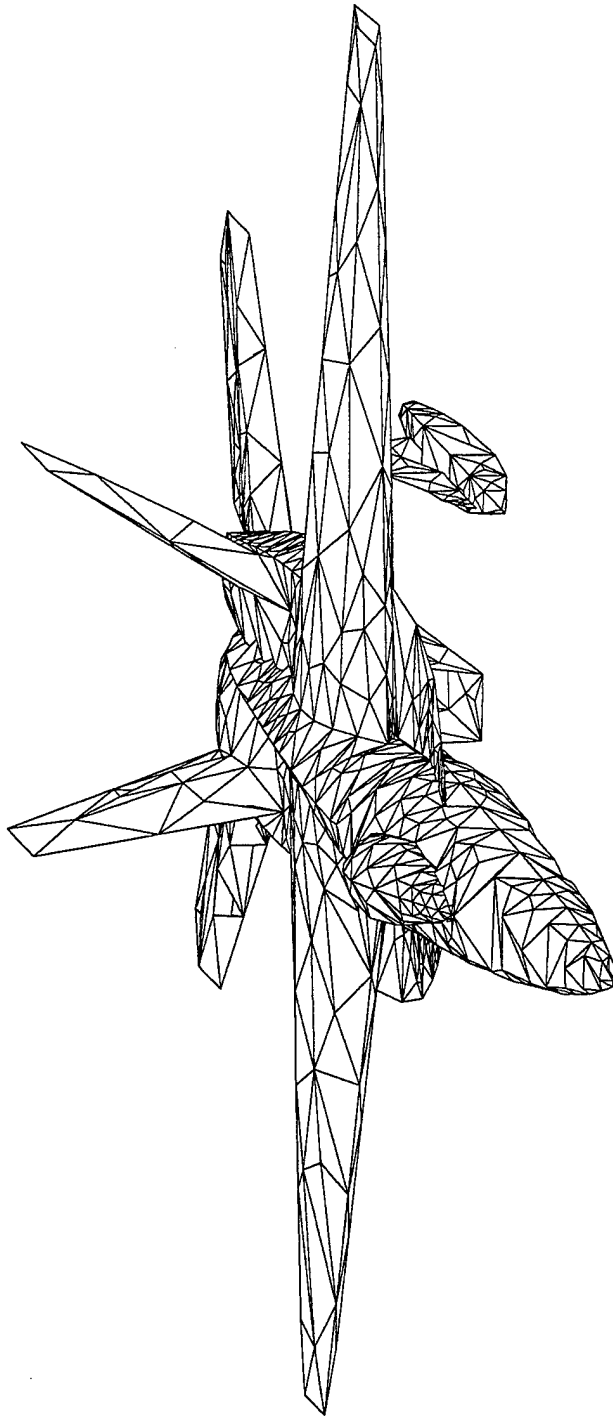


Figure 6: F-18 and CATM facet model built with ACAD (pod at inboard location).

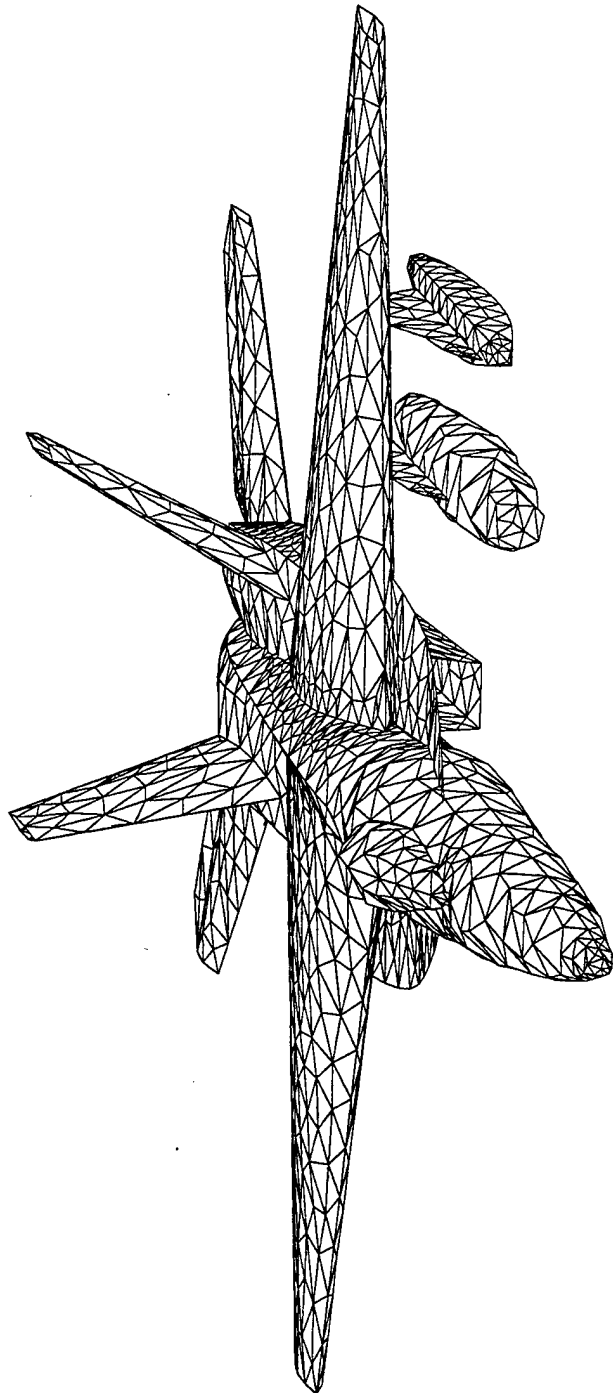


Figure 7: F-18, drop tank, and CATM facet model built with ACAD.

III. ANTENNA MODELS

The first step in evaluating the antenna performance is to construct models of the CATM antennas. The antenna assembly is shown in Figure 8. It consists of a two-turn helix pointed directly aft and two microstrip antennas canted 60 degrees to the right and left sides. The antenna coordinate system is shown in Figure 9. The positive x axis points aft whereas azimuth angle ϕ is measured in the x - y plane in the counterclockwise direction. The convention is to measure azimuth angle in a clockwise direction as on a compass. However, to be consistent with earlier program reports [9], a counterclockwise direction will be used here.

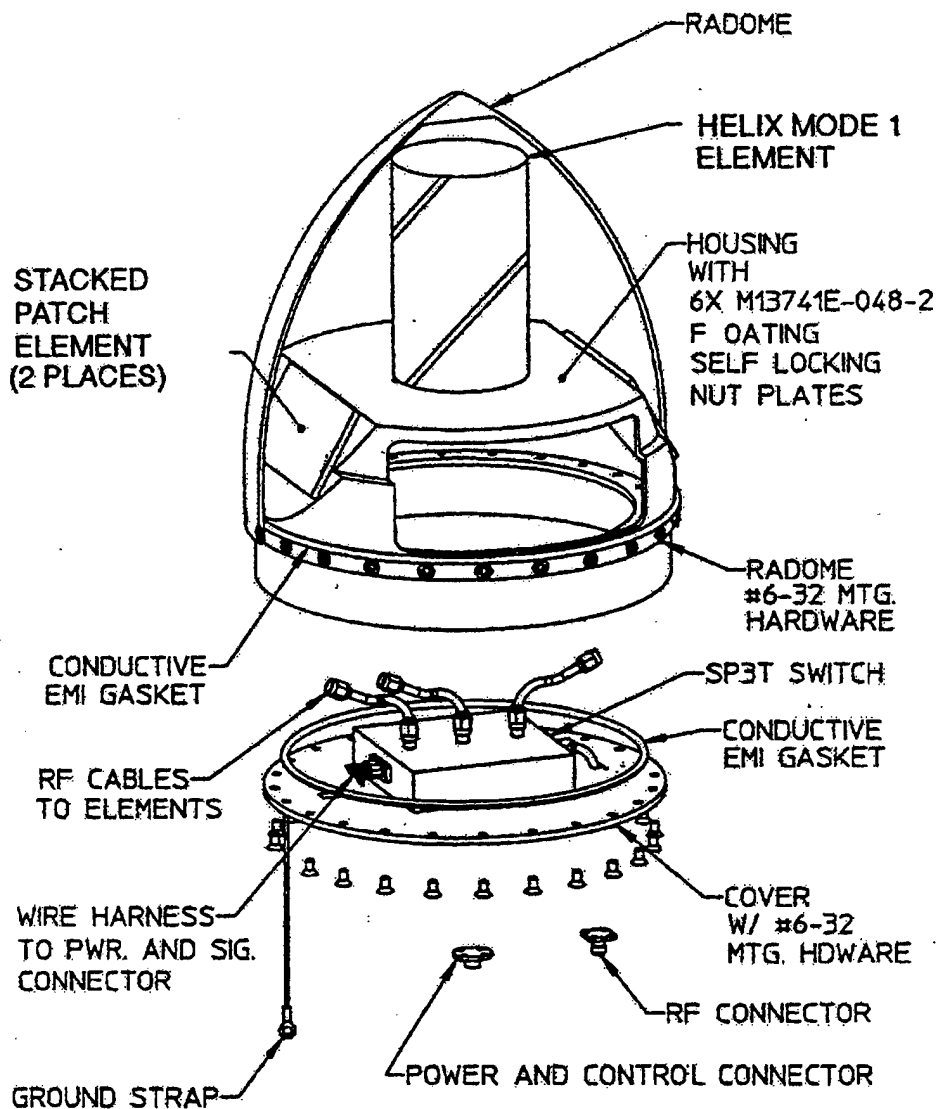


Figure 8: JSOW antenna assembly (From [8]).

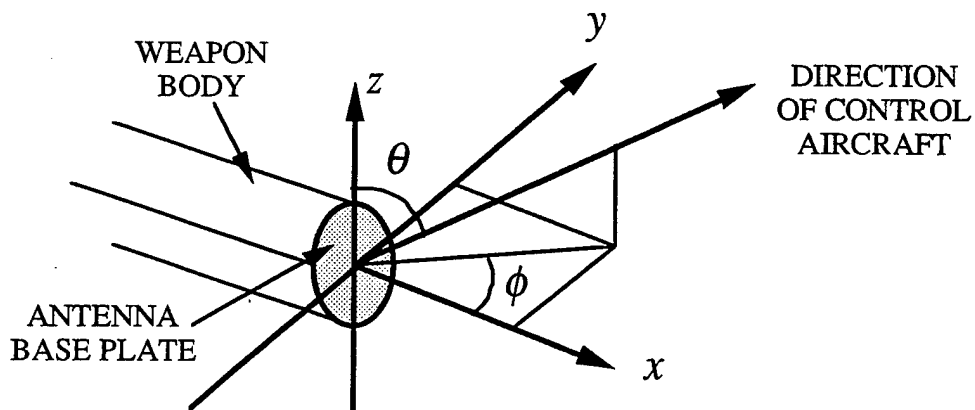


Figure 9: Antenna measurement coordinate system.

The antennas are modeled using the MM code PATCH. An equivalent crossed dipole model was developed that duplicated the measured right-hand and left-hand circularly polarized pattern data, denoted RHCP and LHCP respectively. The antenna is designed to radiate RHCP efficiently. RHCP is also referred to as the co-polarized component; LHCP is the cross-polarized component. A triangular facet model of the antennas is shown in Figure 10.

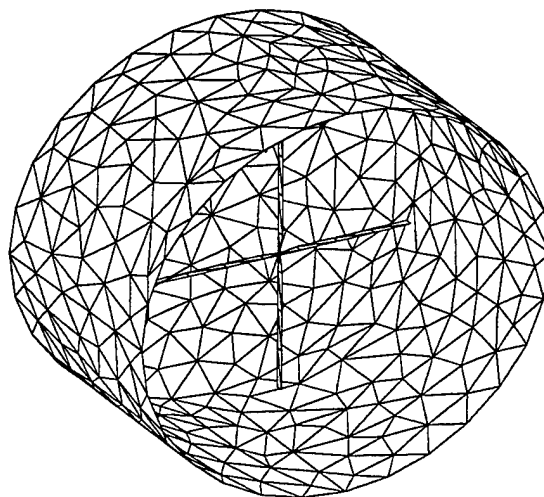


Figure 10: PATCH model used to generate the antenna patterns.

Agreement with measured data was obtained by appropriately scaling the dipole lengths and widths, the height of the dipoles above the cavity base, and the cavity diameter and rim height. Data was generated at three frequencies in the operating band. They will be referred to as the low, mid and high frequencies and designated by the symbols f_L , f_M , and f_H .

Several comparisons between the measured and computed patterns are shown in Figures 11 through 16. Patterns are shown in either a constant azimuth ($AZ=\phi$ a constant) or constant elevation ($EL=\pi/2-\theta$ a constant). Heavy lines signify measured data from [9]; thin lines are calculated data. Solid is used for RHCP and dashed for LHCP. In all cases the agreement between the co-polarized components is good down to about -15 dB relative to the maximum. The agreement for the cross-polarized patterns is generally not as good, and in many cases it is not even available. However, it is the co-polarized patterns that are of interest in this study.

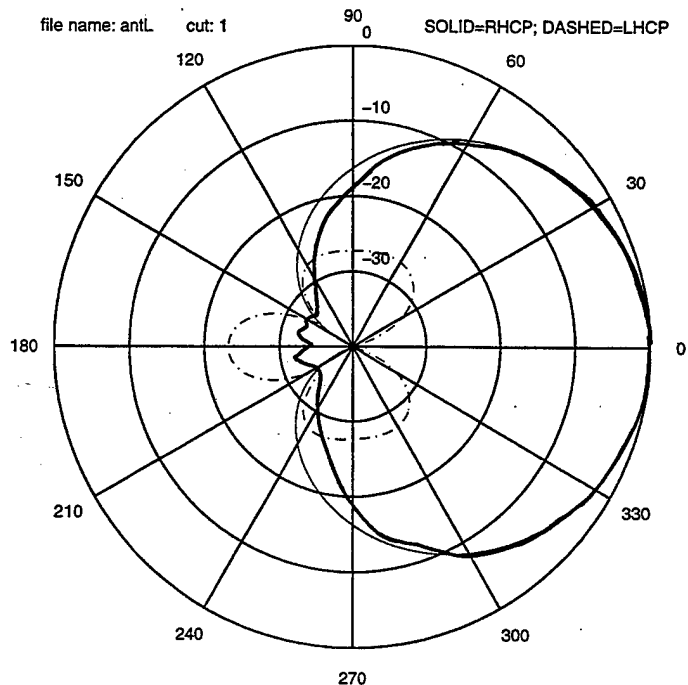


Figure 11: Comparison of measured and calculated helix azimuth pattern at f_L , $EL=0$. (Heavy line: measured; thin line calculated.)

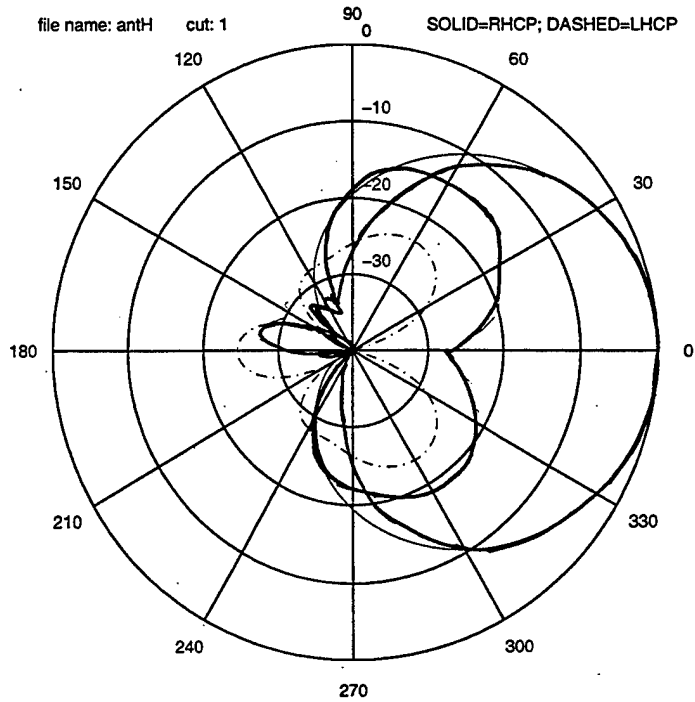


Figure 12: Comparison of measured and calculated helix azimuth pattern at f_H , $EL=0$. (Heavy line: measured; thin line calculated.)

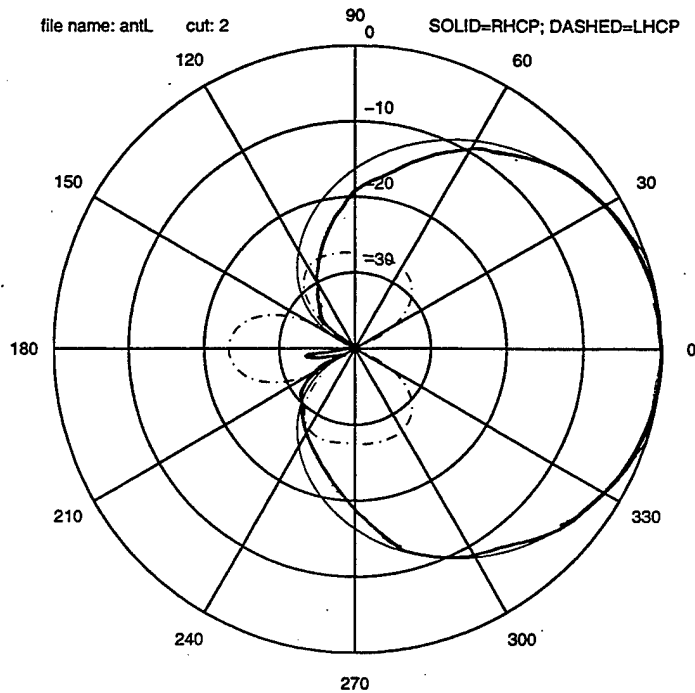


Figure 13: Comparison of measured and calculated helix elevation pattern at f_L , $AZ=0$. (Heavy line: measured; thin line calculate.)

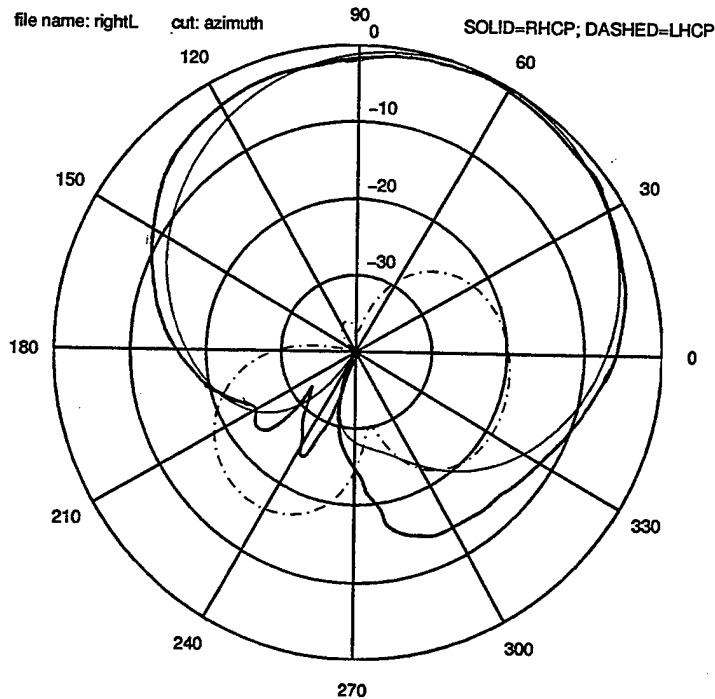


Figure 14: Comparison of measured and calculated microstrip patch azimuth pattern at f_L , $EL=0$. (Heavy line: measured; thin line calculated.)

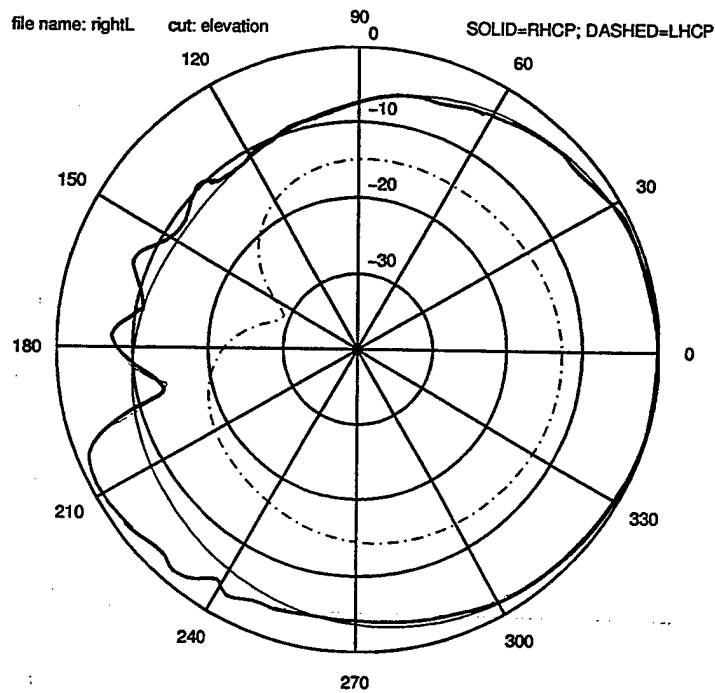


Figure 15: Comparison of measured and calculated microstrip patch elevation pattern at f_L , $AZ=0$. (Heavy line: measured; thin line calculated.)

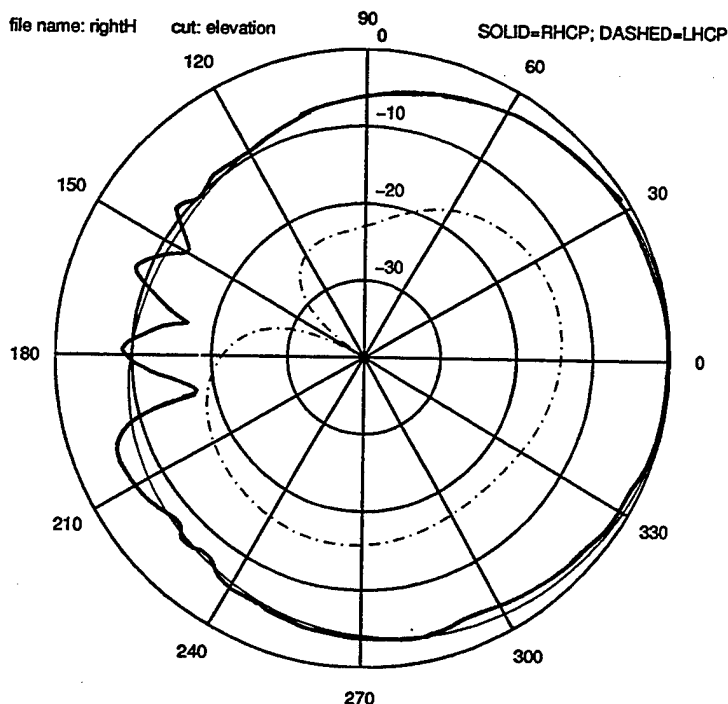


Figure 16: Comparison of measured and calculated microstrip patch elevation pattern at f_H , $AZ=0$. (Heavy line: measured; thin line calculated.)

IV. CAPTIVE CARRY PATTERN CHANGES

A. Description of Calculated Data

Using the radiation patterns computed by the method of moments as a baseline, the changes caused by the carriage aircraft were estimated by comparison of the captive configuration patterns with the baseline patterns. For display purposes a contour plot of the minimum gain contours listed in [9] were included with the calculated patterns. Data was collected for the following cases:

1. CATM mounted on the inboard and outboard locations;
2. Three frequencies: Low, Mid and High;
3. Three antennas: two microstrips and one helix;
4. Drop tank at the inboard location;
5. Short and long CATMs.

The gain contours are plotted as a function of azimuth and elevation. They can be interpreted as angles measured from the antenna to the control aircraft by an observer located at the antenna and facing aft. Examples are:

- a point directly above: $AZ=0$, $EL=+90$
- a point directly below: $AZ=0$, $EL=-90$
- a point to the rear of the aircraft: $AZ=0$, $EL=0$
- starboard (forward facing pilot's right): $AZ=90$, $EL=0$
- port (forward facing pilot's left): $AZ=-90$, $EL=0$

The dashed lines in the figures represent the antenna specification for each particular case. In order to meet the copolarized specification, the dashed contours should be entirely enclosed by the solid (antenna) contours. This is illustrated in the top result in Figure 17 for the isolated antenna. On the other hand, in order to meet the cross-polarized specification, no solid lines should appear inside of the dashed contours. This is illustrated in the bottom of Figure 17. The specific values of the contours are available in [9].

The patterns shown in the following figures are a representative sample of the extensive data collected. A summary of the data presented in the figures is given in Table 4. It lists which figures should be compared in order to observe the effect of the indicated configuration changes.

<u>Configurations</u>	<u>Figures</u>		
	f_L	f_M	f_H
CATM outboard, mode 1	19	20	21
CATM inboard, mode 1	22		23
With drop tank, mode 1	26		27
Short CATM outboard, mode 1	24		
Short CATM inboard, mode 1	25		
Free flight, mode 1	17		18
CATM outboard, mode 2 (outboard antenna)	29, 33		30, 34
CATM outboard, mode 2 (inboard antenna)	31		32
CATM inboard, mode 2 (outboard antenna)	35		
CATM inboard, mode 2 (inboard antenna)	36		
Free flight, mode 2	28		

Table 4: Summary of computed patterns for the various configurations. These are a sample of the complete set of data collected in the study.

B. Mode 1 Data

Mode 1 gain specifications are given in [9]. A comparison of Figures 19 through 27 indicates that there is a loss in gain over a significant part of the quadrant where $-90^\circ \leq AZ \leq 0^\circ$ and $0^\circ \leq EL \leq 90^\circ$. The reason is that the line of sight from the antenna to observation points in this spatial sector are blocked by the F-18 fuselage and tail surfaces. The loss occurs for all

frequencies and CATM configurations, but it is most severe when the CATM is placed at the inboard mount point.

C. Mode 2 Data

The mode 2 specification involves all three antennas, with the wide azimuth angles being covered by the two microstrip antennas which are tilted $\pm 60^\circ$ in azimuth. The contours for the two microstrip antennas are shown in Figure 28. There are two gain values of interest for this mode. The lower level is represented by the rectangular solid line contour and the upper level by the rectangular dash-dot line contour. The center of the gain contours are located at $\pm 60^\circ$ because of the antenna tilts.

The outboard microstrip antenna (which is pointed towards the pilot's left side) is relatively unaffected by the aircraft. This is evident from Figures 29 and 30. On the other hand, the inboard microstrip antenna (which is pointed towards the pilot's right side) is almost completely blocked, as evident from Figures 31 and 32. The gain surfaces for the two antennas are plotted in Figures 33 and 34.

V. CONCLUSIONS

The gain data computed using APATCH indicates that there is significant degradation in the data link between the CATM and the control aircraft due to blockage by the carriage aircraft. The blockage is most serious for the conditions:

- $-90^\circ \leq AZ \leq 0^\circ$ and $0^\circ \leq EL \leq 90^\circ$ for mode 1
- $-90^\circ \leq AZ \leq 0^\circ$ for all elevation angles for the inboard microstrip, mode 2

Changes in the CATM location do not have a dramatic effect on the performance. There is a slight improvement in the mode 1 contours when the CATM is outboard and located as far aft on the pylon as possible. However, there are still some blind sectors when the CATM is on the outboard mount. The inboard microstrip (i.e., the one pointed toward the aircraft fuselage) is blocked at nearly all elevation angles. The outboard microstrip is unaffected by the presence of the aircraft at all elevation angles if $AZ > 0^\circ$.

There are essentially three options available to alleviate the problems associated with the blockage:

1. Restrict the angles for the training so that a clear line of sight is maintained.
2. Use two CATMs, one on each wing, so that there is always a clear line of sight from the control aircraft to one of the

CATMs. This is undesirable because of the cost and weight penalties associated with two CATMs.

3. Use an auxiliary antenna on the side of the aircraft opposite the side where the CATM is mounted. This will require some additional hardware to combine signals or switch between the CATM antennas and the auxiliary antenna.

Another potential problem that arises from the captive configuration is the increase in noise due to the carriage aircraft's exhaust plume [10]. The plume is a high-temperature radiation source that is in the field of view of the control aircraft. This results in an increase in antenna temperature, which leads to decreased signal-to-noise ratio and increased bit error rate. It is expected that this is of second order relative to the effects of antenna gain degradation presented in this report.

VI. REFERENCES

- [1] W. Stutzman and G. Thiele, *Antenna Theory and Design*, Wiley.
- [2] W. A. Johnson, et al, *PATCH Code User's Manual*, Sandia Report SAND87-2991, May 1988.
- [3] D. C. Jenn, "Computer Modeling Techniques for Array Antennas on Complex Structures," Naval Postgraduate School Research Report NPS-EC-97-016, Dec. 1997.
- [4] R. Kipp, et all, *APATCH User's Manual (Version 2.1)*, Demaco, Inc., July 1996.
- [5] R. Marhefka, et all, *Numerical Electromagnetic Code - Basic Scattering Code (NEC BSC): Part I - Users Manual*, ElectroScience Lab, Ohio State University, Tech. Report 712242-14, Dec. 1982.
- [6] C. A. Balanis, *Advanced Engineering Electromagnetics*, Harper and Row, San Francisco, 1982.
- [7] *The ACAD User's Manual*, Lockheed Martin Corp., Ft. Worth, April 1995.
- [8] "Proposal for Joint Standoff Weapon (JSOW) Unitary Program Weapon Data Link (WDL) Antenna E&MD," Ball Telecommunications Products Division, P96-432, Vol.III, Dec. 1966.
- [9] "Critical Item Development Specification for the Unitary Antenna of the Joint Standoff Weapon System," Texas Instruments, U006069E, Oct. 23, 1996 (Secret).
- [10] R. C. Robertson, "Communication Link Considerations," JSOW CATM meeting, 21 May, 1996.

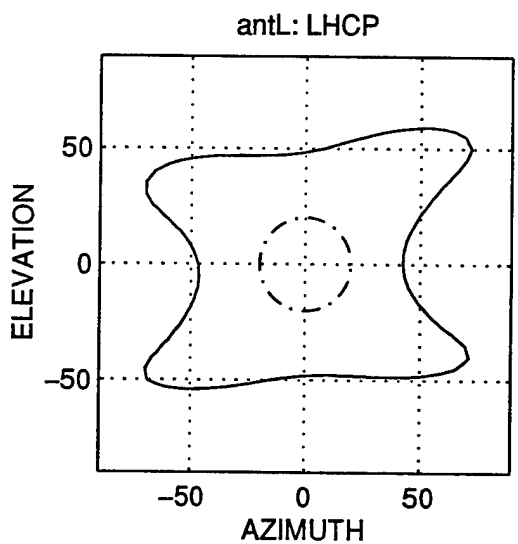
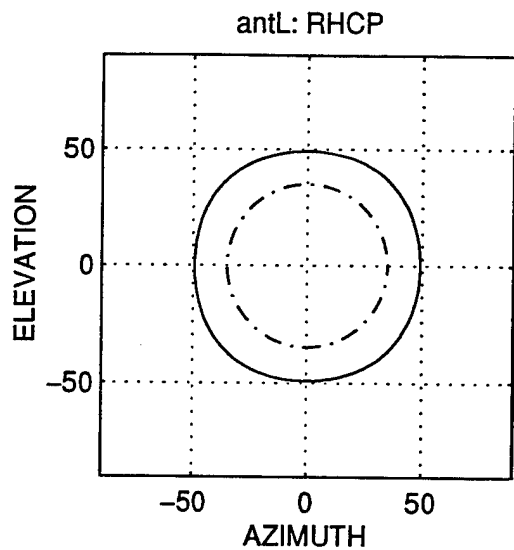


Figure 17: CATM only (no carriage aircraft), low frequency, helix antenna (mode 1).

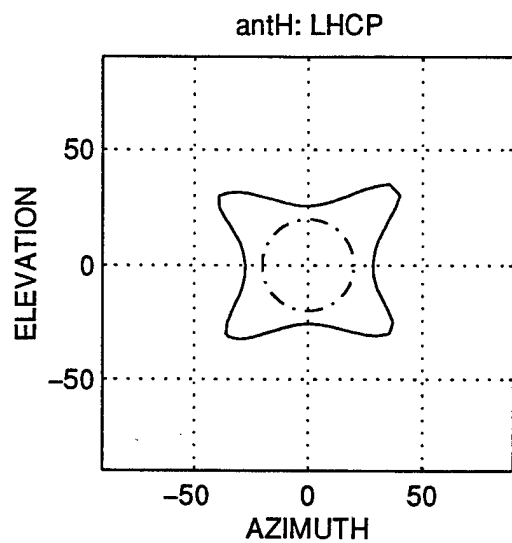
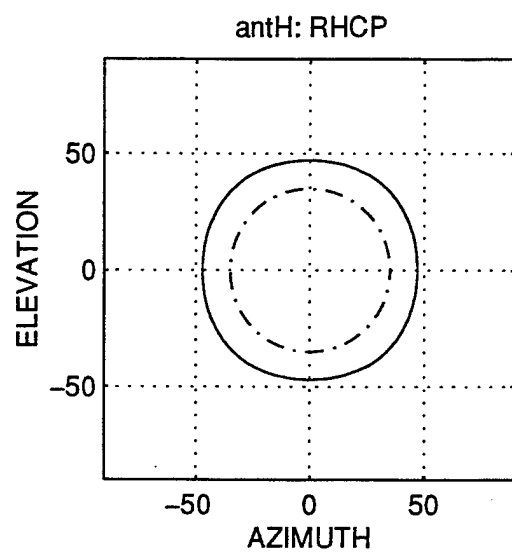


Figure 18: CATM only (no carriage aircraft), high frequency, helix antenna (mode 1).

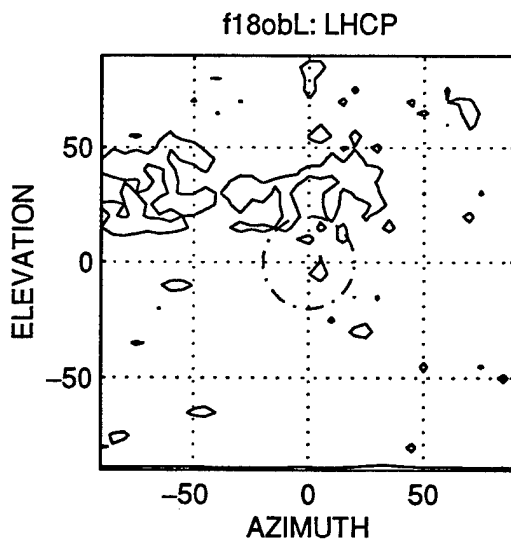
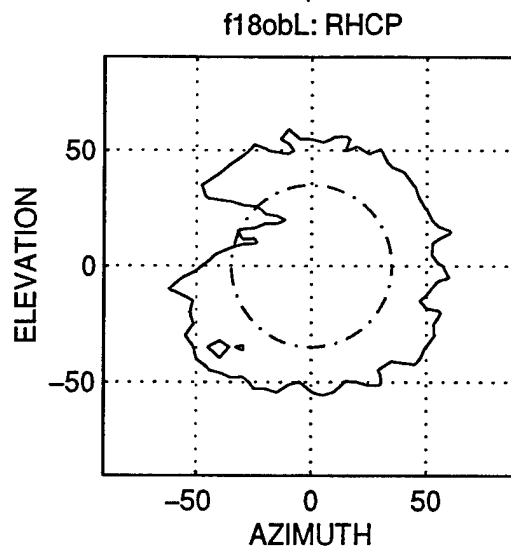


Figure 19: CATM outboard, low frequency, helix antenna (mode 1).

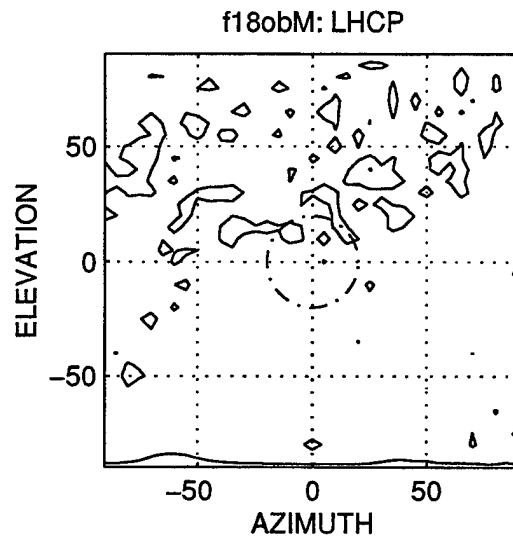
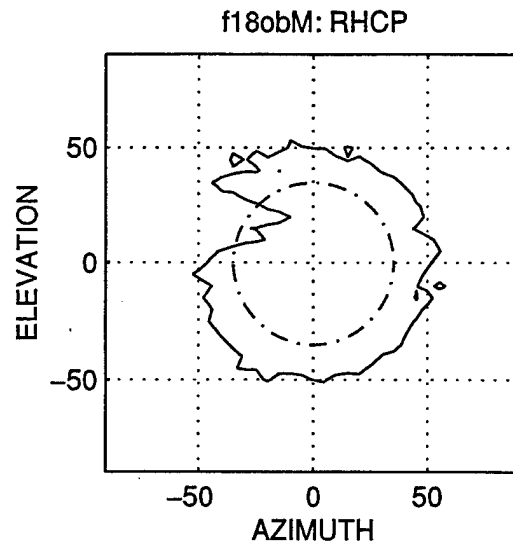


Figure 20: CATM outboard, mid frequency, helix antenna (mode 1).

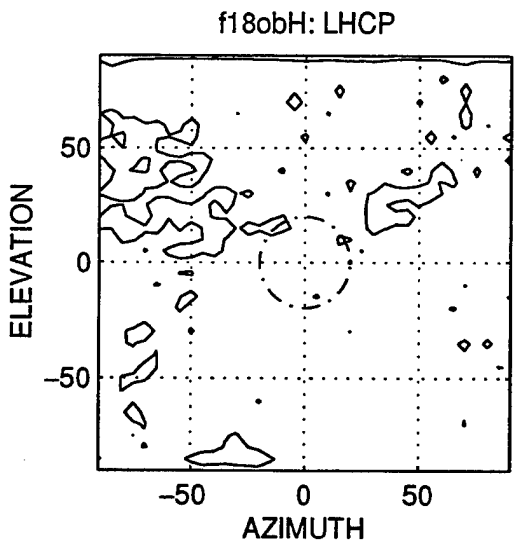
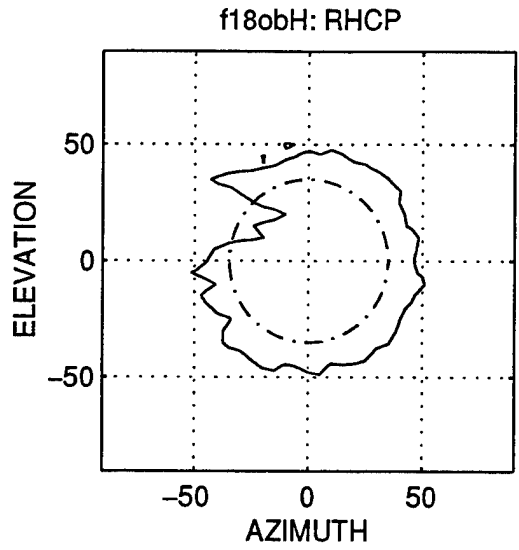


Figure 21: CATM outboard, high frequency, helix antenna (mode 1).

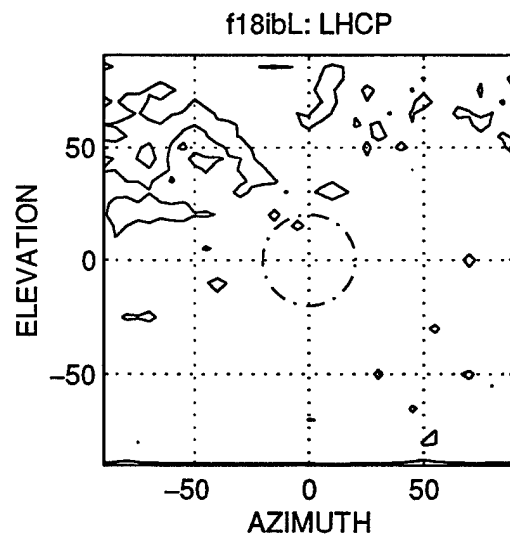
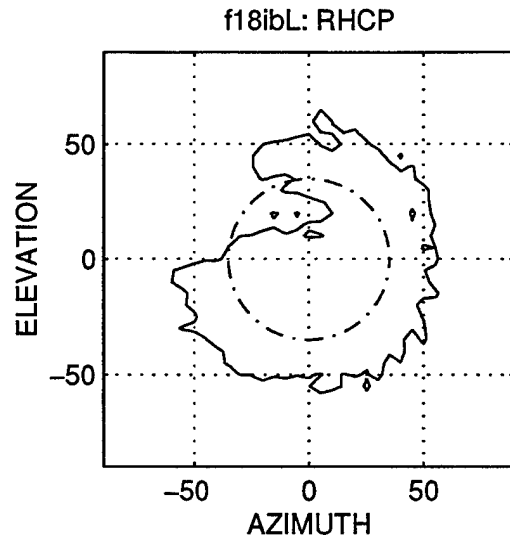


Figure 22: CATM inboard, low frequency, helix antenna (mode 1).

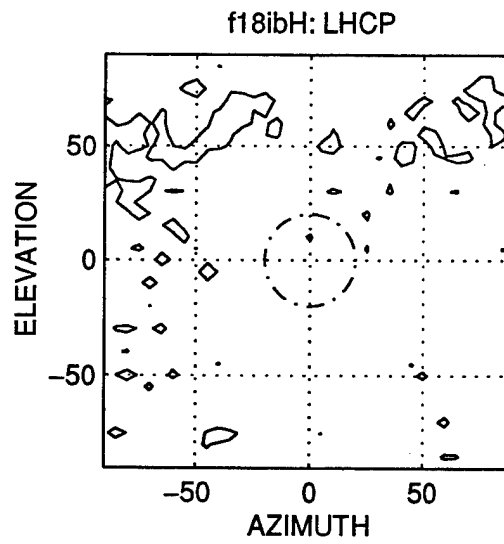
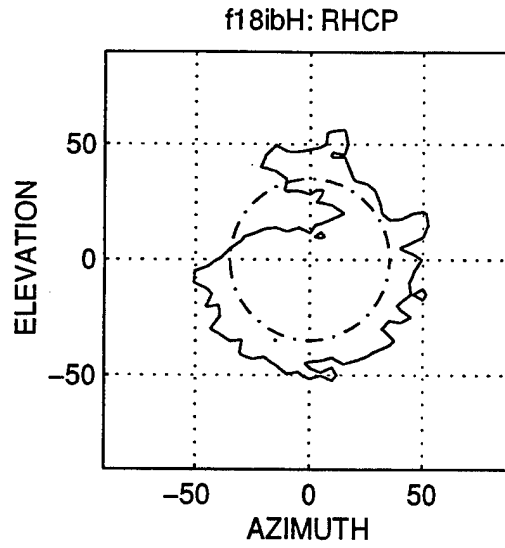


Figure 23: CATM inboard, high frequency, helix antenna (mode 1).

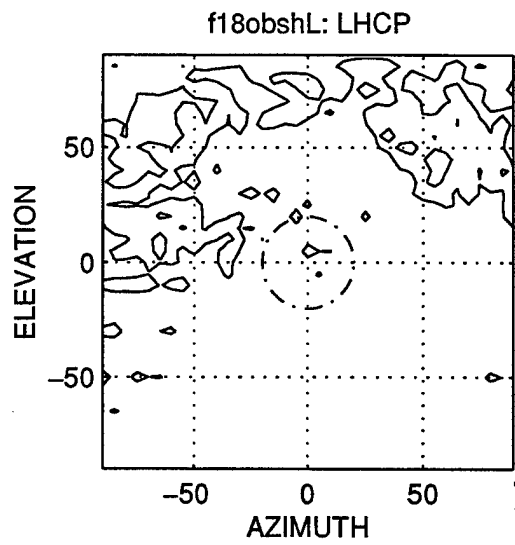
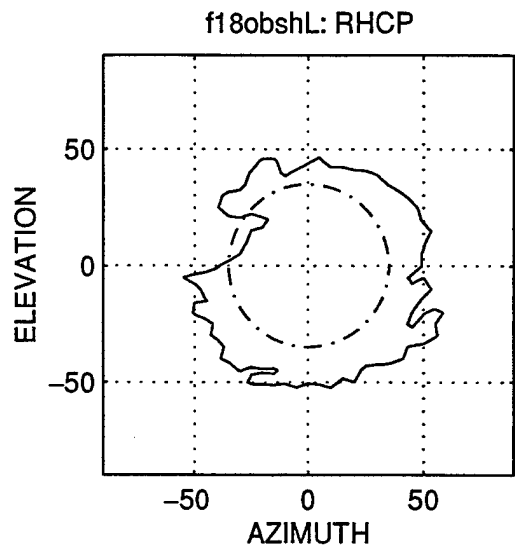


Figure 24: CATM outboard, short configuration, low frequency, helix antenna (mode 1).

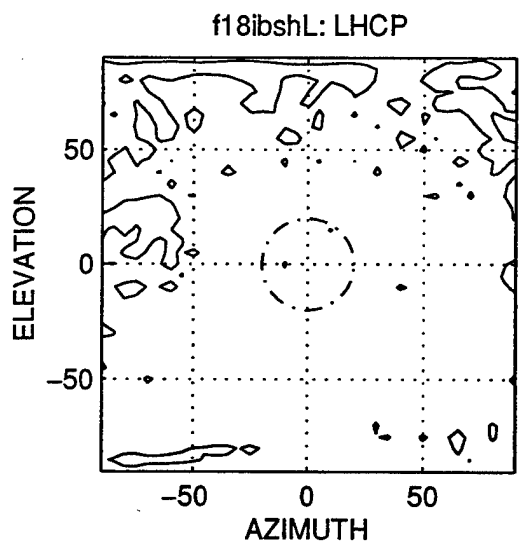
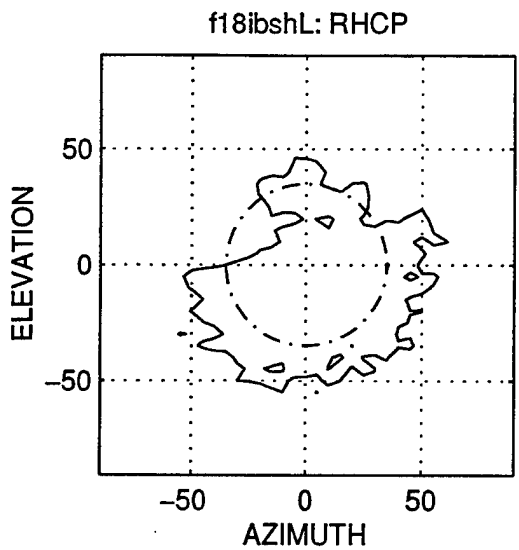


Figure 25: CATM inboard, short configuration, low frequency, helix antenna (mode 1).

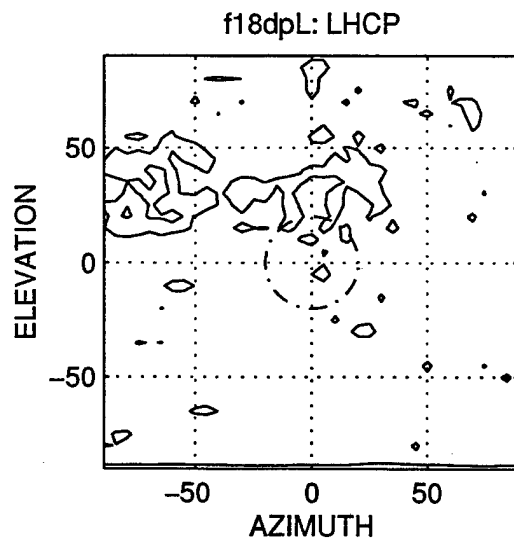
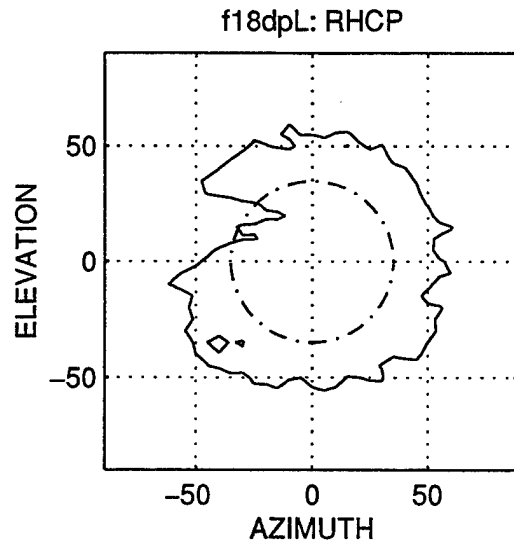


Figure 26: CATM outboard, with drop tank, low frequency, helix antenna (mode 1).

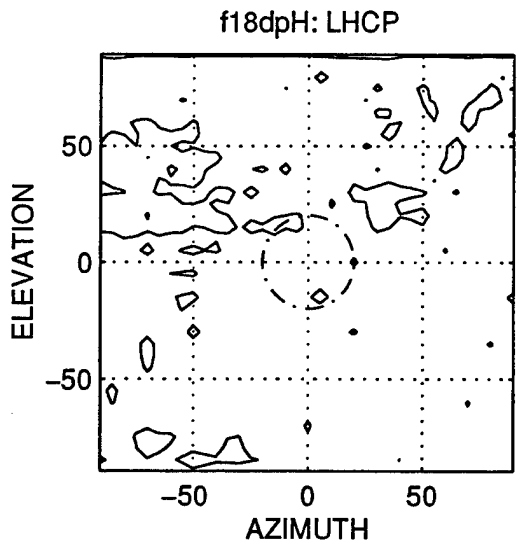
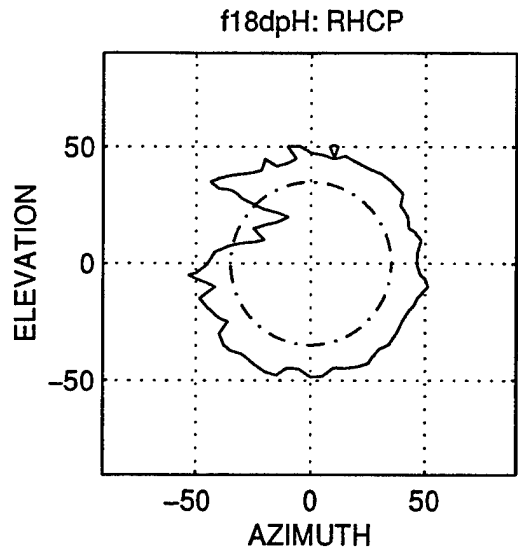


Figure 27: CATM outboard, with drop tank, high frequency, helix antenna (mode 1).

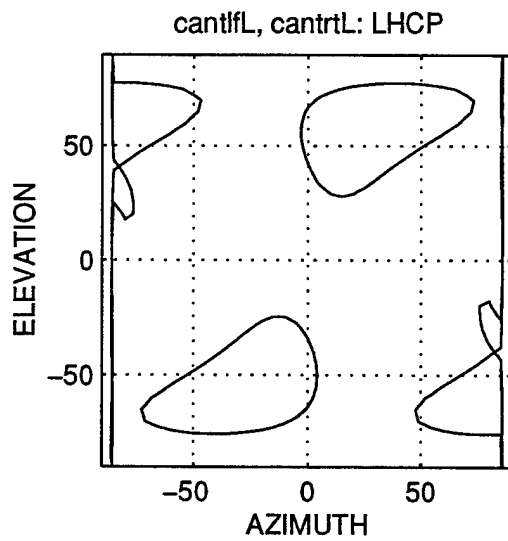
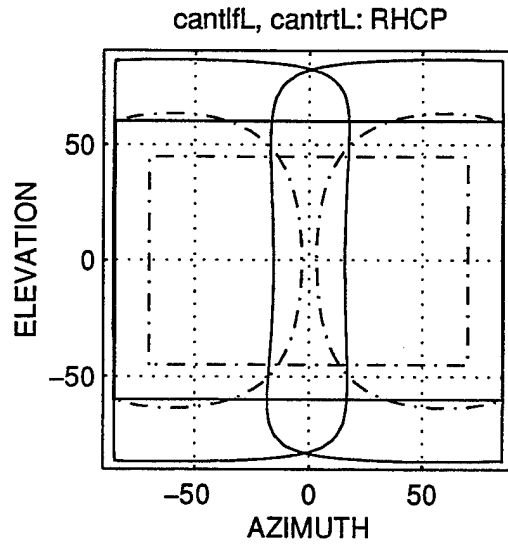


Figure 28: CATM in free flight, low frequency, inboard and outboard microstrip antenna patterns (mode 2).

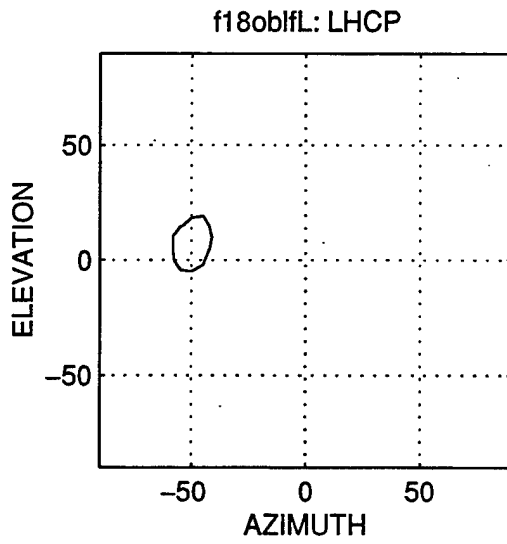
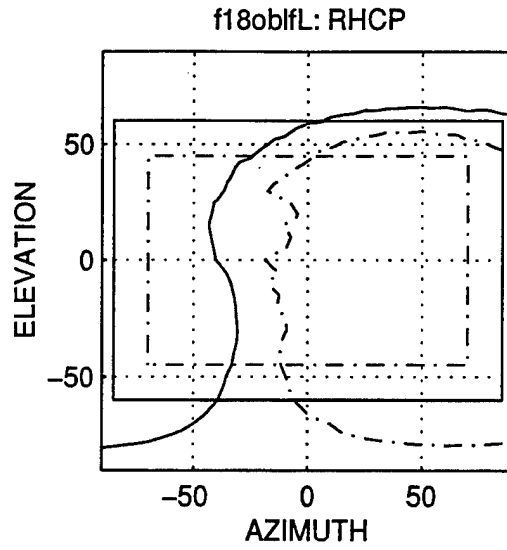


Figure 29: CATM outboard, low frequency, outboard microstrip antenna pattern (mode 2).

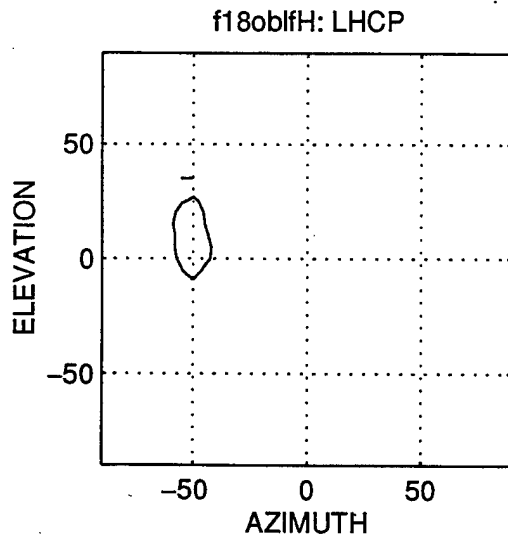
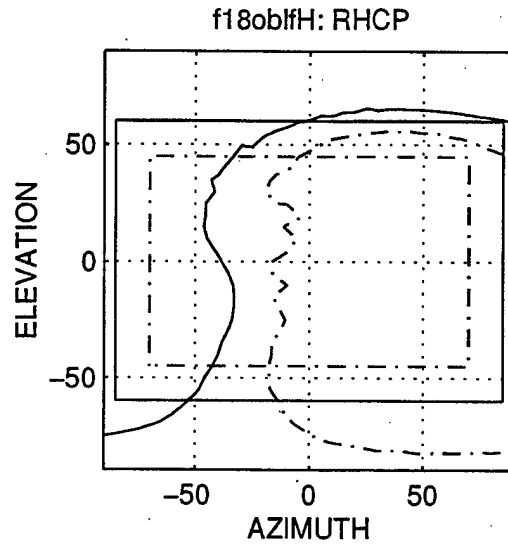


Figure 30: CATM outboard, high frequency, outboard microstrip antenna pattern (mode 2).

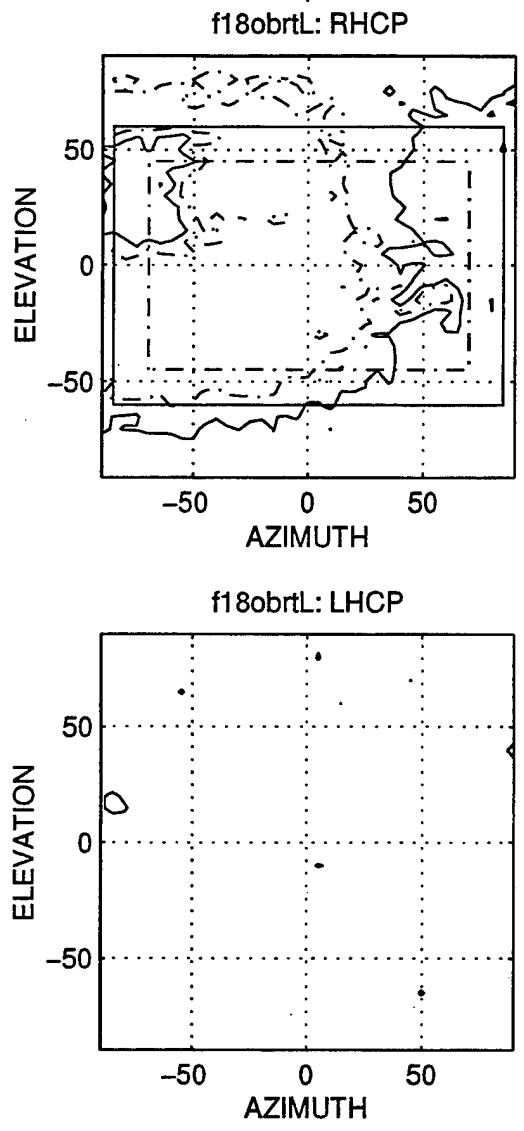


Figure 31: CATM outboard, low frequency, inboard microstrip antenna pattern (mode 2).

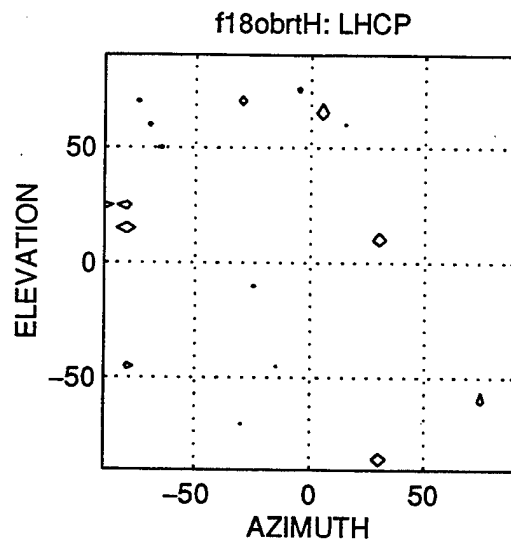
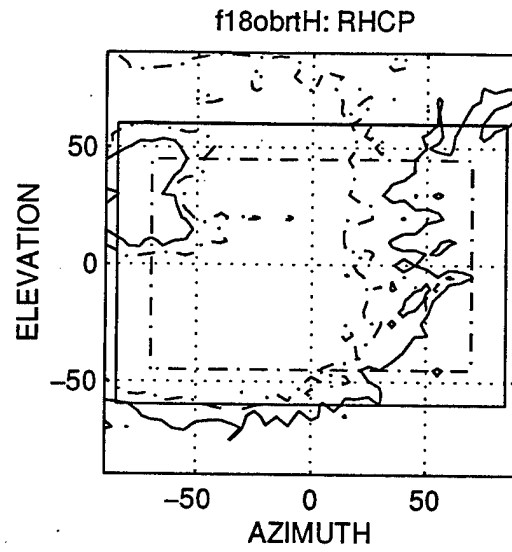


Figure 32: CATM outboard, high frequency, inboard microstrip antenna pattern (mode 2).

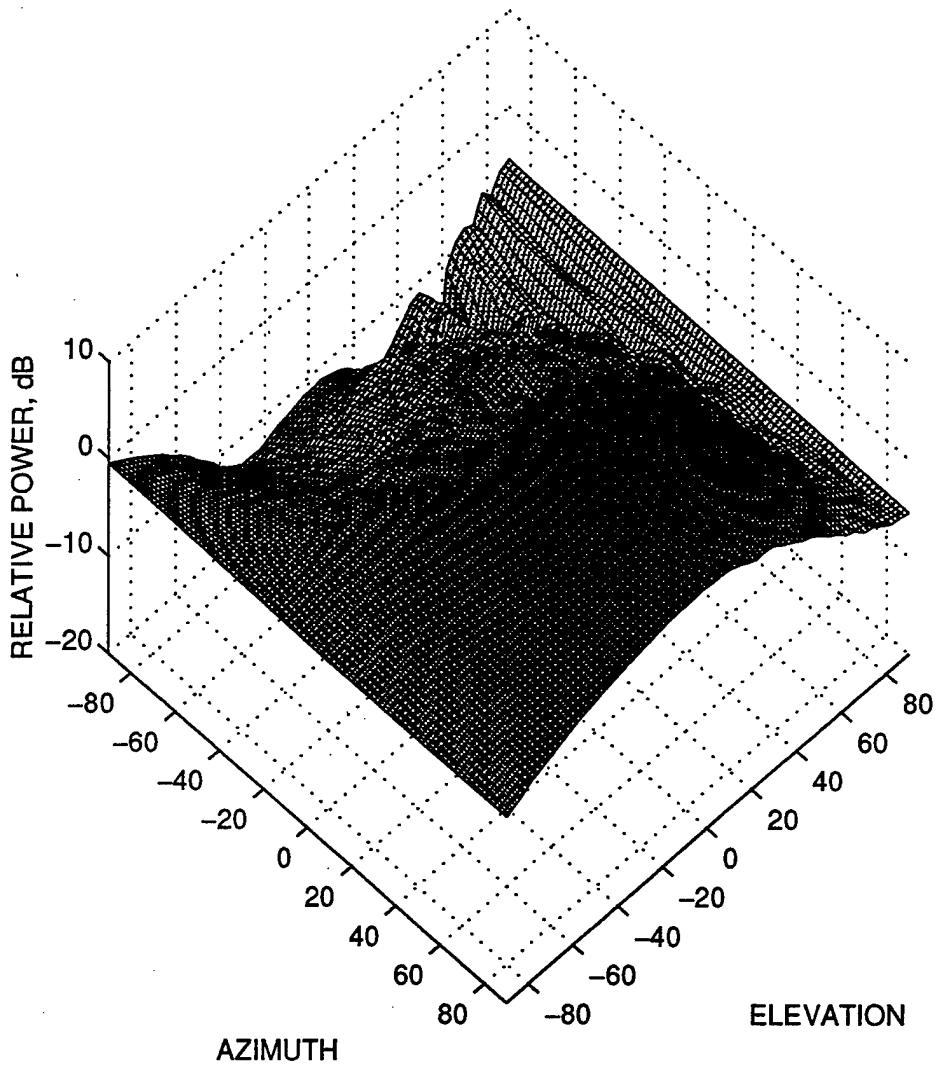


Figure 33: Three dimensional pattern plot for the CATM outboard, low frequency, outboard microstrip antenna pattern (mode 2).

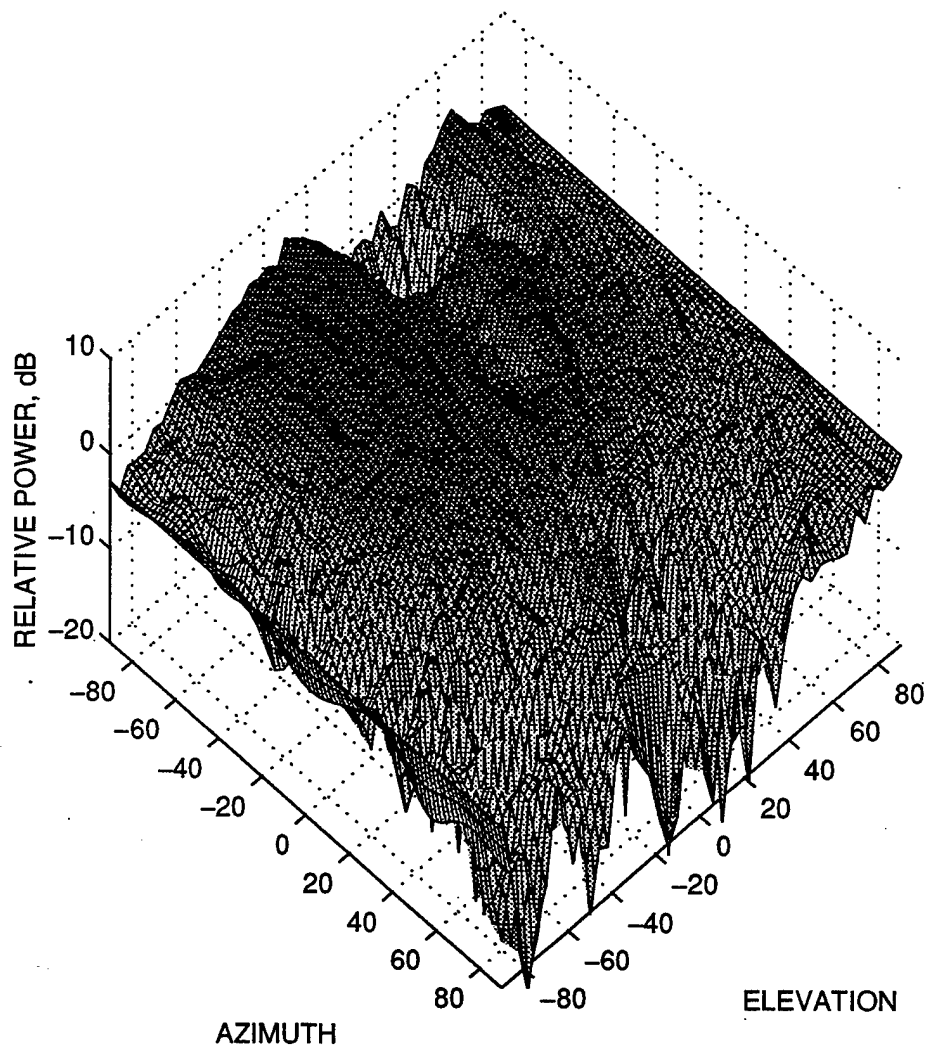


Figure 34: Three dimensional pattern plot for the CATM outboard, low frequency, inboard microstrip antenna pattern (mode 2).

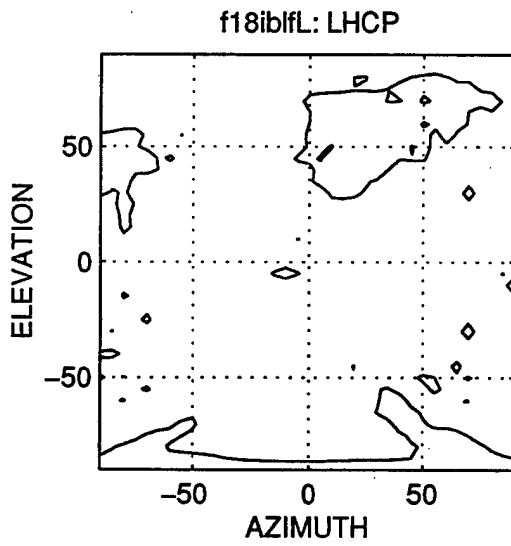
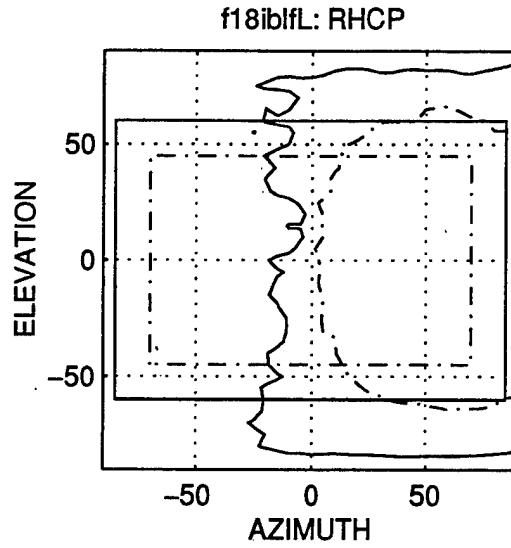


Figure 35: CATM inboard, low frequency, outboard microstrip antenna pattern (mode 2).

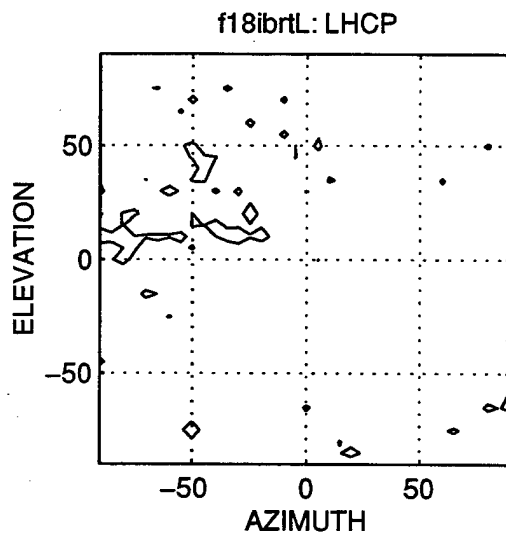
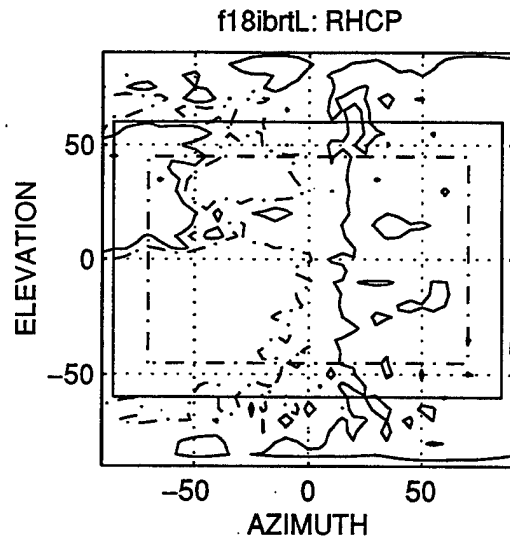


Figure 36: CATM inboard, low frequency, inboard microstrip antenna pattern (mode 2).

INITIAL DISTRIBUTION LIST

	No. Copies
1. Defense Technical Information Center 8725 John J. Kingman Rd, STE 0944 Ft. Belvoir, VA 22060-6218	2
2. Dudley Knox Library, Code 52 Naval Postgraduate School 411 Dyer Road Monterey, CA 93943-5101	2
3. Research Office, Code 09 Naval Postgraduate School 589 Dyer Road Monterey, CA 93943-5138	1
4. Chairman, Code EC Department of Electrical and Computer Engineering Naval Postgraduate School 833 Dyer Road Monterey, CA 93943-5121	1
5. Professor D. C. Jenn, Code EC/Jn Department of Electrical and Computer Engineering Naval Postgraduate School 833 Dyer Road Monterey, CA 93943-5121	2
6. Professor Gerald H. Lindsey, Code AA/Li Department of Aeronautics and Astronautics Naval Postgraduate School 699 Dyer Road Monterey, CA 93943-5106	1
7. Program Executive Officer (TACAIR) Attn: LCDR Mahr, Code PMA-201 Bldg. 2272 Ste 448 47123 Buse Road, Unit IPT Patuxent River, MD 20670-1547	2

- | | No. Copies |
|-----------------------------------------------------------------------------------------------------------------------------------------------------|------------|
| 8. Commanding Officer
Attn: Kurt Reese, Code 471J00D
NAVAIRWPNSTA
1 Administration Circle
China Lake, CA 93555-6100 | 2 |
| 9. Commander
Attn: William Hammersley, Code PMA-201E1, Room 448
COMNAVAIRSYSCOM
47123 Buse Road, Unit IPT
Patuxent River, MD 20670-1547 | 2 |